

Article

A Three-Phase Dynamic Wireless Charging System with Constant Output Voltage

Ruikun Mai , Hongchao Li, Yeran Liu, Kunzhuo Zhou, Ling Fu * and Zhengyou He *

School of Electrical Engineering, Southwest Jiaotong University, Chengdu 610031, China; mairk@swjtu.cn (R.M.); hongchaoli@163.com (H.L.); yeranliu@my.swjtu.edu.cn (Y.L.); kunzhuozhou@163.com (K.Z.)

* Correspondence: lingfu@swjtu.cn (L.F.); hezy@swjtu.cn (Z.H.); Tel.: +86-28-8760-2445 (L.F. & Z.H.)

Received: 7 November 2017; Accepted: 21 December 2017; Published: 1 January 2018

Abstract: A dynamic wireless power transfer (WPT) system is an effective method, which can reduce charging time and extend the driving range of the electric vehicles. In the dynamic WPT systems, the output voltage may fluctuate when the receiver moves along the transmitter coils. This paper proposes a three-phase dynamic WPT charging system with overlapped three-phase transmitter coils. The overlap length is optimized to depress the fluctuation of the output voltage. These coils are powered by a three-phase inverter to generate an even magnetic field, and a unipolar coil is employed as a receiver to simplify the coil structure of the secondary side. Based on the proposed three-phase coil structure, the output voltage characteristics of the system are analyzed in detail. A 500 W dynamic charging prototype is established to validate the proposed dynamic charging system. Experimental results show that the output voltage fluctuation is within $\pm 3.05\%$. The maximum system efficiency reaches 89.94%.

Keywords: wireless power transfer; three-phase inverter; dynamic charging

1. Introduction

Internal combustion engine vehicles, the most prevailing transportation in past decades, contribute to the undesired emission of global greenhouse gas, spurring research into electric vehicles (EVs) and the smart grid [1]. The wireless power transfer (WPT) has many advantages compared with wired charger technology (e.g., opportunity charging, safety, immunity to ice, water, spark and other chemicals), [2,3] which makes WPT an ideal charging implementation in mobile phones, pacemakers and underwater robots [4,5].

WPT systems mainly focus on stationary charging applications such as medical implants [6], household appliances and stationary EVs [7]. In a stationary EVs charging situation, the vehicle is required to park in the designated position, and the receiver coil should be well-aligned with the transmitter coil, which is worrisome [8]. Also, the battery limits the cruising range of the vehicles and needs to be frequently recharged. Although a huge battery increases the cruising range, the system suffers from increased weight, longer charging time and higher cost. Besides, frequent fast charging and deep discharging of batteries degrade the lifespan of the expensive onboard batteries [9,10].

The dynamic WPT system can solve these issues mentioned above. When the vehicle is moving on the track, it can be recharged continuously. Thus, the cruising range of the EV can be extended, and the weight and cost of the vehicles can be reduced with a small battery. The total length of the transmitter is 90 m in a 3460 m route in Korea [11,12], and the maximum charging power reaches 100 kW [13]. This system has few circuit components and a simple structure, but the maximum efficiency of the system is only about 74% at 27 kW output [14]. In [15,16], multiple short transmitters are arranged on the lane of the vehicle, and the system is flexible for design and installation. However, it requires a great quantity of compensation components, and the output power reduces to almost zero between two transmitters

due to the existence of a dead point [17]. A novel T-type compensation network is proposed in [18], which keeps a stable transmission power. Apart from the methods mentioned above, the design of coil structures is another useful method to reduce the output power fluctuation for the dynamic WPT system. Circular coils are adopted to charge electrical vehicle when the vehicles move along the track [19]. However, the output power diminishes at the border of two adjacent coils. To solve this issue, a three-phase bipolar WPT system is adopted in [20], which can create a broader power delivery zone than a single-phase track. The switchable transmitter coils are adopted in [21]. To keep the coupling of the transmitters and receiver, the geometry of the receiver is optimized. A prototype is set up for medium power transfer (tens of Watts). A novel array-type coils design is presented to overcoming the coil misalignment in [22] for the static charging. In [23], a homogeneous wireless power transfer system is proposed. The alternate transmitter coils are utilized to enhance the magnetic field density. The paper mainly focuses on the coupling between the transmitter coils. In order to balance the three-phase currents, the system had to add additional compensation. The fluctuation of output power is almost $\pm 20\%$. In [24], both the transmitters and the receiver are using the LCC network. The inter-coupling between adjacent coils are investigated in detail. The maximal value of output power is about three times larger than the minimal value of output power. To reduce the fluctuation of magnetic fields along the track, the coils are arranged closely in [25]. The mutual inductance between transmitter coils is compensated by extra capacitors.

This paper is mainly focused on the suppression of the fluctuation by optimizing the overlap of the transmitter coils, which is not taken into account by the aforementioned research. Six transmitter coils are adopted to form a track, and all the coils are powered by a three-phase inverter. Each transmitter coil has its own compensation circuits, and different transmitter coils are connected in parallel. The overlap of the adjacent transmitter coils and the circuit parameters are designed to minimize the output voltage fluctuations. Theoretical analysis has been experimentally verified, and the output voltage fluctuation is within $\pm 3.05\%$ of the average voltage.

This paper is organized as follows: Section 2 describes the optimization of transmitter coils arrays. Section 3 analyzes the output voltage based on the fundamental harmonic model of dynamic WPT system. The proposed design is validated by experiments in Section 4. The conclusion is drawn in Section 5, finally.

2. Design and Optimization of Coil Structure

For the dynamic charging systems, the transmitter coils are usually arranged in an array [11,12]. The mutual inductance between the transmitter coil and the receiver coil varies with the position of the receiver coil. Accordingly, the induced voltage of the receiver coil varies with the fluctuation of mutual inductance.

The coil structure of the dynamic charging system is depicted in Figure 1. Six square unipolar coils are arranged closely on the ferrite plates. The size of a single square coil is l .

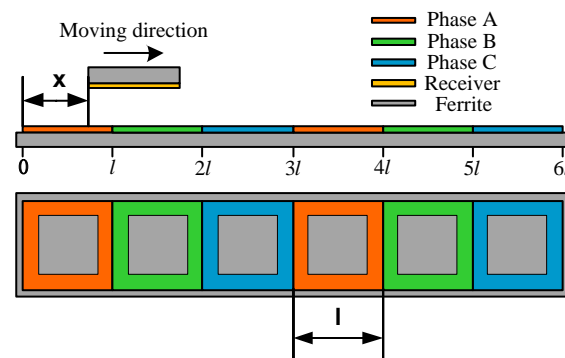


Figure 1. Structure of the transmitters and receiver.

The equivalent circuit for the three-phase system is shown in Figure 2. The phasors of the induced voltages \dot{V}_{AS} , \dot{V}_{BS} and \dot{V}_{CS} in the receiver can be expressed as:

$$\begin{cases} \dot{V}_{AS} = j\omega M_{AS} \dot{I}_{TA} \\ \dot{V}_{BS} = j\omega M_{BS} \dot{I}_{TB} \\ \dot{V}_{CS} = j\omega M_{CS} \dot{I}_{TC} \end{cases} \quad (1)$$

where ω is the angular frequency of the system, and \dot{I}_{TA} , \dot{I}_{TB} and \dot{I}_{TC} are the phasors of the current in transmitter A, B and C, respectively. Therefore, the sum of induced voltage on the receiver side is as follows:

$$\dot{V}_S = j\omega M_{AS} \dot{I}_{TA} + j\omega M_{BS} \dot{I}_{TB} + j\omega M_{CS} \dot{I}_{TC} \quad (2)$$

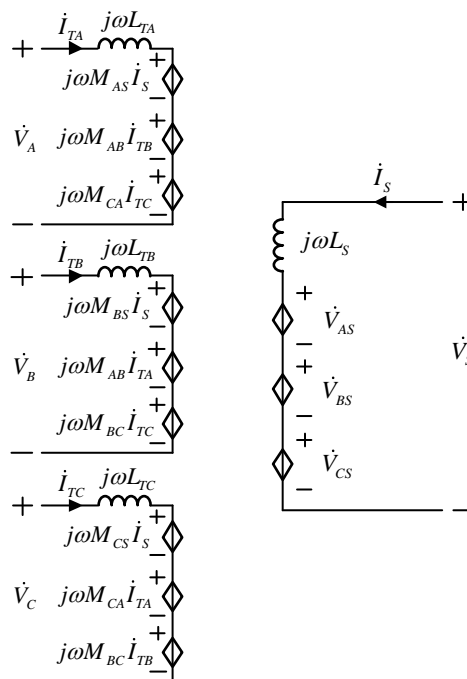


Figure 2. Circuit topology of the proposed coil structure.

The mutual inductance between the transmitter and receiver coils is calculated using a 3-D FEA tool, ANSYS Maxwell (Ozen Engineering, Inc., Silicon Valley, CA, USA). The specifications in simulation and experiment are listed in Table 1. x is defined as the relative position between the transmitter and receiver. The simulated mutual inductance between the transmitter and receiver coils is shown in Figure 3.

Table 1. Parameters of the transmitter and the receiver.

Parameters	Value
Length of a Q coil [26] l /mm	200
Air gap distance l_G /mm	70
Q coil turns in transmitter A N_A	17
Q coil turns in transmitter B N_B	17
Q coil turns in transmitter C N_C	17
Q coil turns in receiver N_R	17
Relative position x /mm	[0,1200]

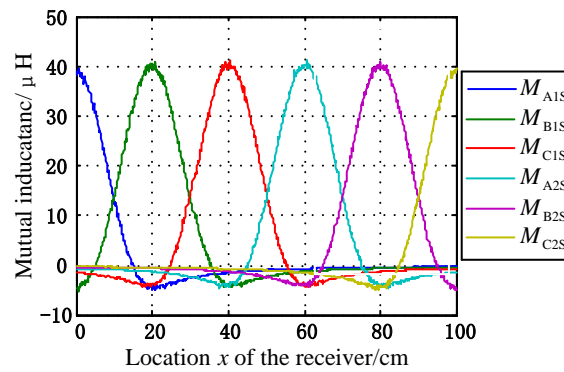


Figure 3. Simulated mutual inductance between the receiver and transmitters.

Assuming that the amplitude of each coil current is equal. The relationship between \dot{I}_{TA} , \dot{I}_{TB} and \dot{I}_{TC} can be expressed as:

$$\begin{cases} \dot{I}_{TA} = I_{T0} \angle 0^\circ \\ \dot{I}_{TB} = I_{T0} \angle 120^\circ \\ \dot{I}_{TC} = I_{T0} \angle 240^\circ \end{cases} \quad (3)$$

where I_{T0} is the RMS value of the current in the transmitter coil. The amplitude $|\dot{V}_S|$ of the induced voltage can be expressed as:

$$\begin{aligned} |\dot{V}_S| &= |j\omega M_{AS} I_{TA} + j\omega M_{BS} I_{TB} + j\omega M_{CS} I_{TC}| \\ &= |j\omega I_{T0} (M_{AS} + M_{BS} e^{j\frac{2}{3}\pi} + M_{CS} e^{j\frac{4}{3}\pi})| \end{aligned} \quad (4)$$

F_M is the sum of all mutual inductances:

$$F_M = M_{AS} + M_{BS} e^{j\frac{2}{3}\pi} + M_{CS} e^{j\frac{4}{3}\pi} \quad (5)$$

The Equation (4) shows that the amplitude of the induced voltage $|\dot{V}_S|$ is related to F_M directly, when ω and I_{T0} are constant.

The mutual inductances against the location of the receiver and F_M calculated by Equation (5) are shown in Figure 4. Large fluctuation of F_M exists with the given parameters, which will lead to the fluctuation of the induced voltage. In order to alleviate the fluctuation of F_M , overlapping is employed, which is depicted in Figure 5. The overlap length is defined as L_O .

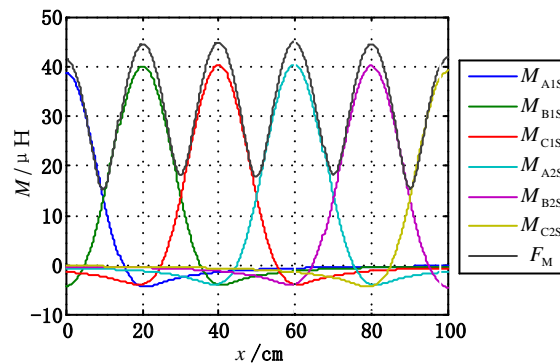


Figure 4. Processed mutual inductance.

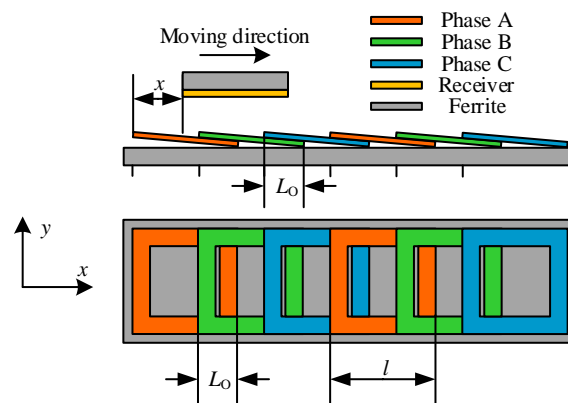


Figure 5. Illustration of the transmitters and receiver after overlapping.

From the Figure 6, the fluctuation of F_M varies as per the overlap of coils. It is of importance to find the optimal overlap length to minimize the fluctuation of F_M . The variance $D(F_M)$ is used to measure the fluctuation of F_M , when the receiver moves from the second transmitter coils to the fifth transmitter coils. The variance of F_M with various overlapped length is calculated and shown in Figure 7.

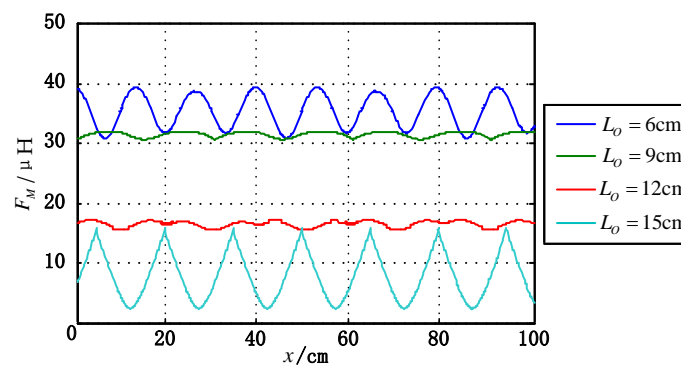


Figure 6. The sum of mutual inductance with different overlapped length.

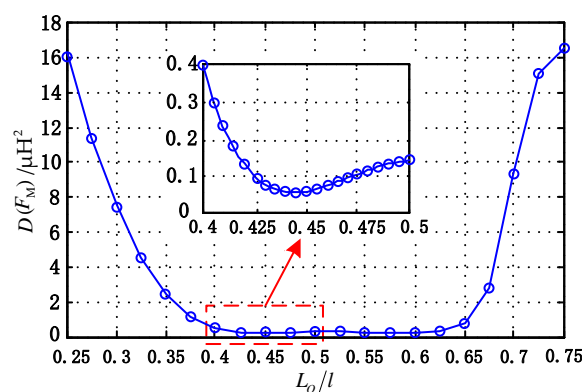


Figure 7. Variance with various overlap proportion.

$D(F_M)$ is the square of the standard deviation of F_M . As shown in Figure 7, $D(F_M)$ varies with the overlap proportion of the coil length, and the smallest variance occurs when L_0/l is about 0.45. The calculated variance reaches the smallest value when the overlap proportion is 0.445 from the

details of Figure 7. Meanwhile, the fluctuation of F_M is the minimum, and the induced voltage is nearly uniform versus the variation of x .

According to the analysis, the induced voltage is dependent on the sum of all mutual inductances. The fluctuation of F_M and the voltage can be reduced by overlapping three-phase transmitter coils.

The fluctuation of F_M is robust to the movement of the receiver along the x direction, but is affected by the misalignment between the transmitter coils and the receiver coil along the y direction as shown in Figure 5. Considering the misalignment along the y direction, the mutual inductances is simulated by ANSYS Maxwell, and F_M is calculated. The calculated results are shown in Figure 8 where L_{dis} indicates the lateral displacement of the receiver along the y direction. The mutual inductances between the transmitters and the receiver will decrease with the increment of L_{dis} . The fluctuation of F_M is still constant, but smaller than that with no misalignment, when the receiver moves along the track.

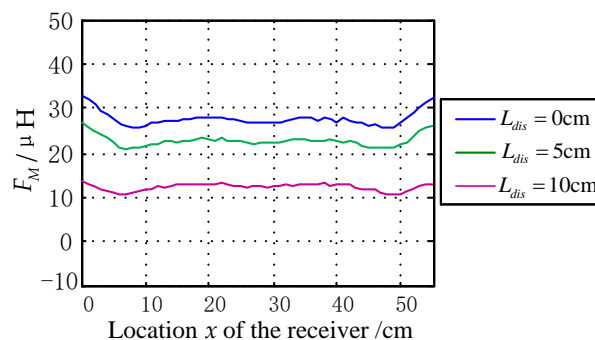


Figure 8. The sum of mutual inductance considering misalignment along the y direction.

3. Circuit Analysis

The circuit topology of the dynamic WPT system is shown in Figure 9. The input of the system is a direct current (DC) source V_{dc} , which is connected to a three-phase full-bridge inverter to apply three high-frequency ac voltage v_{PA} , v_{PB} and v_{PC} to the resonant circuit. The LCC networks [24,25] are chosen as the resonant compensation topologies for the transmitters. Each transmitter coil is compensated independently. There are transmitter coil L_{TA} (L_{TB} , L_{TC}), resonant compensation inductors L_{PA} (L_{PB} , L_{PC}), and resonant capacitors C_{PA} (C_{PB} , C_{PC}) and C_{TA} (C_{TB} , C_{TC}) in each transmitter side. A series resonant compensation, consisting of L_S and C_S , is adopted on the receiver side. M_{AS} , M_{BS} and M_{CS} are the mutual inductances between the transmitter coils and receiver coil. M_{AB} , M_{BC} and M_{CA} are the mutual inductances between the transmitter coils.

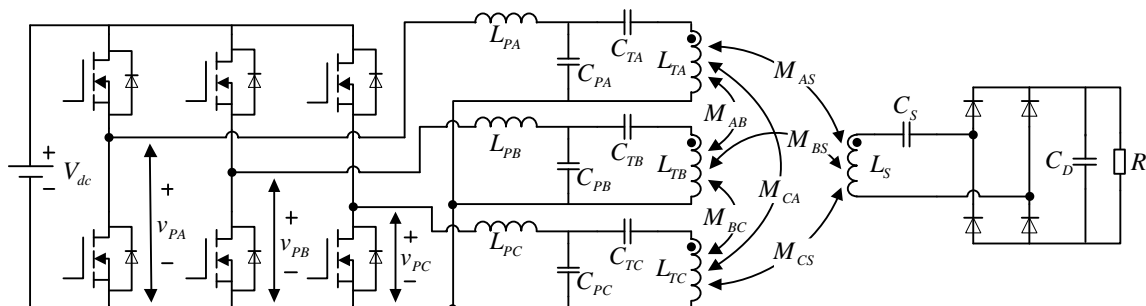


Figure 9. Schematic of the proposed system.

The fundamental harmonics approximation method is used to analyze the circuit shown in Figure 10. The inverter is regarded as first-order harmonic voltage sources. R_{TA} (R_{TB} , R_{TC}) and R_S are the equivalent series resistors of the transmitter coil A (B, C) and the receiver coil respectively.

The rectifier and the dc load resistor R can be represented as an equivalent AC load resistor R_{Leq} [27], which is defined as:

$$R_{Leq} = \frac{8R}{\pi^2} \tag{6}$$

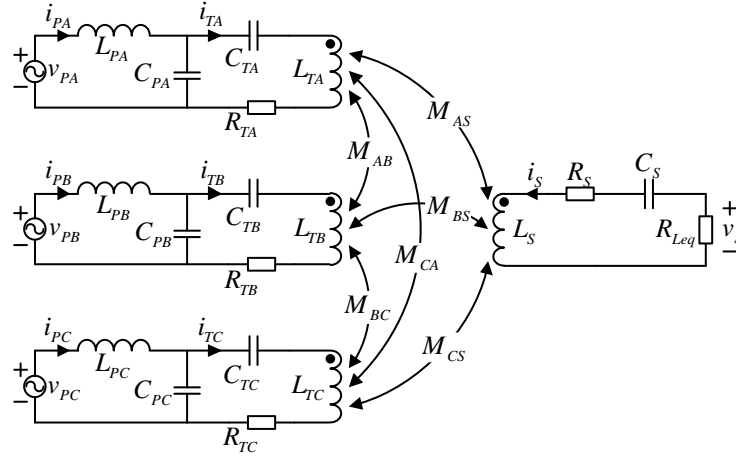


Figure 10. Equivalent circuit of the proposed system.

$Z_{PA1}(Z_{PB1}, Z_{PC1})$ and $Z_{PA2}(Z_{PB2}, Z_{PC2})$ are the circuit impedance of the A (B, C)-phase in transmitter side. The circuit impedance of receiver side is Z_S which is defined as:

$$\left\{ \begin{array}{l} Z_{PA1} = j\omega L_{PA} + 1/j\omega C_{PA} \\ Z_{PA2} = 1/j\omega C_{TA} + j\omega L_{TA} + R_{TA} + 1/j\omega C_{PA} \\ Z_{PB1} = j\omega L_{PB} + 1/j\omega C_{PB} \\ Z_{PB2} = 1/j\omega C_{TB} + j\omega L_{TB} + R_{TB} + 1/j\omega C_{PB} \\ Z_{PC1} = j\omega L_{PC} + 1/j\omega C_{PC} \\ Z_{PC2} = 1/j\omega C_{TC} + j\omega L_{TC} + R_{TC} + 1/j\omega C_{PC} \\ Z_S = j\omega L_S + R_S + 1/j\omega C_S + R_{Leq} \end{array} \right. \tag{7}$$

Each transmitter circuit parameters of the three-phase dynamic charging system are the same. Thus, the relationship is expressed as:

$$\left\{ \begin{array}{l} L_{PA} = L_{PB} = L_{PC} \\ C_{PA} = C_{PB} = C_{PC} \\ C_{TA} = C_{TB} = C_{TC} \\ L_{TA} = L_{TB} = L_{TC} \\ R_{TA} = R_{TB} = R_{TC} \end{array} \right. \tag{8}$$

The values of C_{PA} , C_{TA} and C_S are designed by:

$$\left\{ \begin{array}{l} C_{PA} = \frac{1}{\omega^2 L_{PA}} \\ C_{TA} = \frac{1}{\omega^2 [L_{TA} - 1/(\omega^2 C_{PA})]} \\ C_S = \frac{1}{\omega^2 L_S} \end{array} \right. \tag{9}$$

Based on the Kirchhoff's voltage law, the system can be expressed as:

$$\begin{bmatrix} \dot{V}_{PA} \\ 0 \\ \dot{V}_{PB} \\ 0 \\ \dot{V}_{PC} \\ 0 \\ 0 \end{bmatrix} = \begin{bmatrix} Z_{PA1} & -j/\omega C_{PA} & 0 & 0 & 0 & 0 & 0 \\ -j/\omega C_{PA} & Z_{PA2} & 0 & j\omega M_{AB} & 0 & j\omega M_{CA} & j\omega M_{AS} \\ 0 & 0 & Z_{PB1} & -j/\omega C_{PB} & 0 & 0 & 0 \\ 0 & j\omega M_{AB} & -j/\omega C_{PB} & Z_{PB2} & 0 & j\omega M_{BC} & j\omega M_{BS} \\ 0 & 0 & 0 & 0 & Z_{PC1} & -j/\omega C_{PC} & 0 \\ 0 & j\omega M_{CA} & 0 & j\omega M_{BC} & -j/\omega C_{PC} & Z_{PC2} & j\omega M_{CS} \\ 0 & j\omega M_{AS} & 0 & j\omega M_{BS} & 0 & j\omega M_{CS} & Z_S \end{bmatrix} \begin{bmatrix} \dot{I}_{PA} \\ \dot{I}_{TA} \\ \dot{I}_{PB} \\ \dot{I}_{TB} \\ \dot{I}_{PC} \\ \dot{I}_{TC} \\ \dot{I}_S \end{bmatrix} \quad (10)$$

The induced voltage in the receiver can be calculated from Equation (10) as:

$$\begin{aligned} \dot{V}_S &= -R_{Leq} \times \dot{I}_S \\ &= \frac{8R(\dot{V}_{PA}M_{AS} + \dot{V}_{PB}M_{BS} + \dot{V}_{PC}M_{CS})}{L_{PA}(8R + \pi^2R_S)} \end{aligned} \quad (11)$$

where \dot{V}_{PA} , \dot{V}_{PB} and \dot{V}_{PC} are the output voltages of the three-phase inverter. The relationship between \dot{V}_{PA} , \dot{V}_{PB} and \dot{V}_{PC} can be shown as:

$$\begin{cases} \dot{V}_{PB} = \dot{V}_{PA}e^{j\frac{2}{3}\pi} \\ \dot{V}_{PC} = \dot{V}_{PA}e^{j\frac{4}{3}\pi} \end{cases} \quad (12)$$

By substituting Equation (12) into Equation (11), the induced voltage can be derived as:

$$\dot{V}_S = \frac{8R\dot{V}_{PA}(M_{AS} + M_{BS}e^{j\frac{2}{3}\pi} + M_{CS}e^{j\frac{4}{3}\pi})}{L_{PA}(8R + \pi^2R_S)} \quad (13)$$

Considering Equations (5) and (13), the output voltage \dot{V}_S is related to F_M , when the R , L_{PA} and \dot{V}_{PA} are constant. Consequently, the fluctuation of output voltages reaches the minimum value with minimal fluctuation of F_M .

It should be noted that the angle frequency of the system is fixed and is equal to that of the inverter. Except for the generation of pulse width modulation (PWM) waves of the three-phase inverter, there's no extra measurement circuit or control loop which is easy for implementation for practice.

4. Experimental Verification

A 500 W system is established to validate the proposed dynamic charging system as shown in Figure 11. All of the six transmitter coils have the same shape. Each transmitter coil with its compensation circuit is connected with a three-phase inverter in parallel. A square coil works as a receiver. The size and shape of each coil is identical as that described in Section 2. Six transmitter coils share a three-phase inverter. The air gap distance in the dynamic charging system is 70 mm. The rectifier and the compensation circuit of receiver coil are connected to a dc load resistor. The circuit parameters of the experimental system are listed in Table 2.

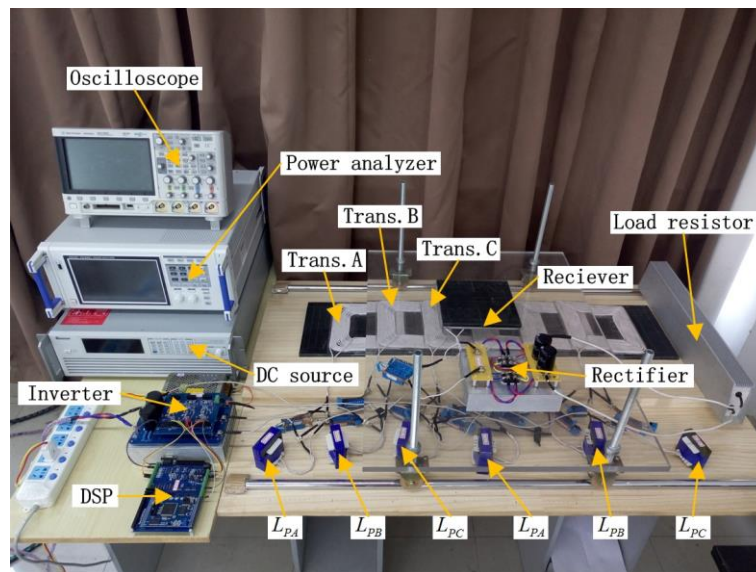


Figure 11. Experimental prototype.

Table 2. Parameters of the experiment system.

Parameters	Value	Parameters	Value
f/kHz	200	R_{TB}/Ω	0.15
V_{dc}/V	315	$L_{PC}/\mu\text{H}$	50.29
V_{out}/V	72	C_{PC}/nF	12.94
L_O/cm	8.9	$L_{TC}/\mu\text{H}$	119.47
$L_{PA}/\mu\text{H}$	50.39	C_{TC}/nF	15.32
C_{PA}/nF	12.36	R_{TC}/Ω	0.1
$L_{TA}/\mu\text{H}$	120.1	$L_S/\mu\text{H}$	110.53
C_{TA}/nF	14.98	C_S/nF	5.96
R_{TA}/Ω	0.1	R_S/Ω	0.18
$L_{PB}/\mu\text{H}$	49.6	Maximum value of $M_{AS}/\mu\text{H}$	37.68
C_{PB}/nF	13.73	Maximum value of $M_{BS}/\mu\text{H}$	38.1
$L_{TB}/\mu\text{H}$	122.8	Maximum value of $M_{CS}/\mu\text{H}$	38.55
C_{TB}/nF	13.95	Output capacitor $C_D/\mu\text{F}$	940

A three-phase inverter is used to provide an ac excitation at the primary side. The oscilloscope Agilent DSO-X 3014T (Keysight Technologies, Beijing, China) is used to recording waveforms, and the efficiency between dc source and dc load is gauged by the power analyzer HIOKIPW6001 (HIOKI, Tokyo, Japan). When the receiver position $x = 644$ mm, the stable waveforms of the output voltage v_{PC} of the three-phase inverter, the output current i_{PC} of the three-phase inverter, the input voltages u_{rec} and the input current i_S of the rectifier are illustrated in Figure 12.

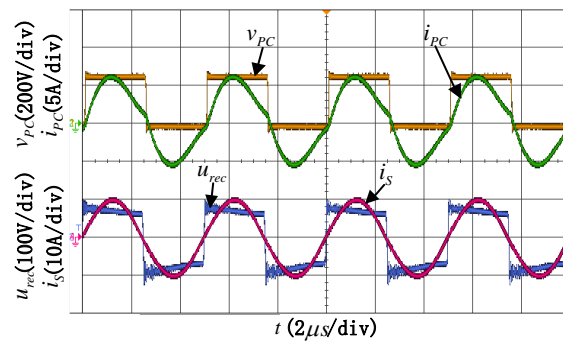


Figure 12. Stable waveforms of the output voltages and currents of inverter and rectifier.

In Figure 13a, is aligned with transmitter coil L_{TC} . M_{CS} is much larger than M_{AS} and M_{BS} . Therefore, i_{PC} is much larger than the other two, where i_{PA} and i_{PB} are almost equal. As the receiver moves to the transmitter coil L_{TA} , the i_{PA} increases gradually and the i_{PC} is gradually reduced which is shown in Figure 13b,c.

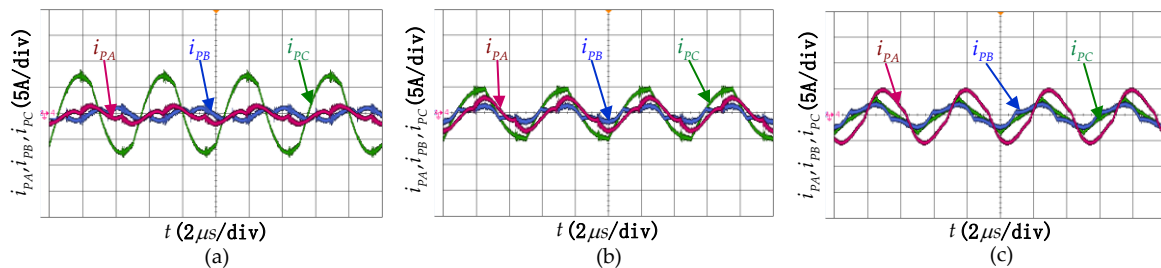


Figure 13. Measured the input current of inverter waveforms. (a) Waveforms with $x = 222$ mm; (b) waveforms with $x = 259$ mm; (c) waveforms with $x = 296$ mm.

When the receiver moves along the transmitters track, the system output voltage and efficiency are shown in Figure 14. The system output voltage stays about 72 V with a fluctuation of $\pm 3.05\%$. The highest system efficiency between the dc source and the dc load reaches up to 89.94% and the lowest efficiency is 86.67%. In [28], the system output power fluctuation is about $\pm 5.89\%$ with a load resistance of 50Ω , and the maximum of the output power is 230 W. The verification system’s maximum output power is around 120 W in [29]. The maximum efficiency is 84% and the fluctuation of power is more than $\pm 50\%$.

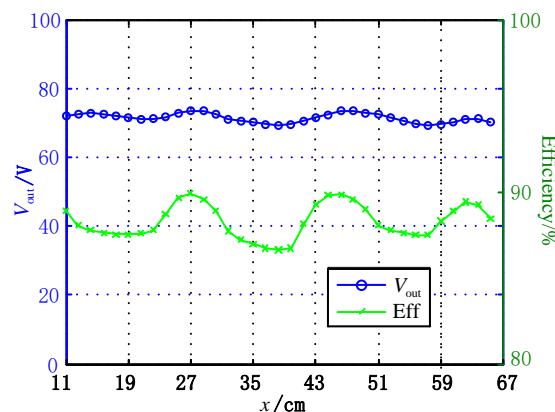


Figure 14. System output voltage and efficiency with various receiver positions.

5. Conclusions

Aimed at reducing the voltage fluctuations in a dynamic WPT system, a three-phase dynamic charging system with two closely arranged overlapping transmitter coils to eliminate voltage dips between coils is proposed in this paper. The overlap length is optimized to reduce the fluctuation of the output voltage. The LCC-S compensation network is adopted in this paper. A 500 W output power dynamic charging system is set up to validate the proposed method. The experimental results show that the fluctuation of system output voltage is $\pm 3.05\%$. The system's highest efficiency from dc source to dc load reaches 89.94%.

Acknowledgments: This paper was supported by National Key R&D Program of China (2017YFB1201002), the National Natural Science Foundation of China under Grant (No. 51677155), the Sichuan Youth Science & Technology Foundation (No. 2016JQ0033), the Fundamental Research Funds for the Central Universities (No. 2682017QY01).

Author Contributions: Ruikun Mai and Ling Fu designed the methodology and wrote the manuscript. Hongchao Li and Yeran Liu conceived and designed the experiments. Hongchao Li and Kunzhuo Zhou implemented the experiments. All authors contributed to improving the quality of the manuscript.

Conflicts of Interest: The authors declare no conflict of interest.

References

1. Yilmaz, M.; Krein, P.T. Review of Battery Charger Topologies, Charging Power Levels, and Infrastructure for Plug-in Electric and Hybrid Vehicles. *IEEE Trans. Power Electron.* **2013**, *28*, 2151–2169. [[CrossRef](#)]
2. Li, Y.; Mai, R.; Lin, T.; Sun, H.; He, Z. A Novel WPT System Based on Dual Transmitters and Dual Receivers for High Power Applications: Analysis, Design and Implementation. *Energies* **2017**, *10*, 174. [[CrossRef](#)]
3. Aditya, K.; Williamson, S. Linearization and Control of Series-Series Compensated Inductive Power Transfer System Based on Extended Describing Function Concept. *Energies* **2016**, *9*, 962. [[CrossRef](#)]
4. Keeling, N.A.; Covic, G.A.; Boys, J.T. A Unity-Power-Factor IPT Pickup for High-Power Applications. *IEEE Trans. Ind. Electron.* **2010**, *57*, 744–751. [[CrossRef](#)]
5. Qiang, H.; Huang, X.; Tan, L.; Ji, Q.; Zhao, J. Achieving Maximum Power Transfer of Inductively Coupled Wireless Power Transfer System Based on Dynamic Tuning Control. *Sci. China Technol. Sci.* **2012**, *55*, 1886–1893. [[CrossRef](#)]
6. Xue, R.; Cheng, K.; Je, M. High-Efficiency Wireless Power Transfer for Biomedical Implants by Optimal Resonant Load Transformation. *IEEE Trans. Circuits Syst. I Regul. Pap.* **2013**, *60*, 867–874. [[CrossRef](#)]
7. Wu, H.H.; Gilchrist, A.; Sealy, K.D.; Bronson, D. A High Efficiency 5 kW Inductive Charger for EVs Using Dual Side Control. *IEEE Trans. Ind. Inform.* **2012**, *8*, 585–595. [[CrossRef](#)]
8. Deng, J.; Lu, F.; Li, W.; Ma, R.; Mi, C. Zvs Double-Side LCC Compensated Resonant Inverter with Magnetic Integration for Electric Vehicle Wireless Charger. In Proceedings of the 2015 IEEE Applied Power Electronics Conference and Exposition (APEC), Charlotte, NC, USA, 15–19 March 2015; pp. 1131–1136.
9. Buchmann, I. Fast and Ultra-Fast Chargers, 2017. Fast and Ultra-Fast Chargers—Battery University. Available online: http://batteryuniversity.com/learn/article/ultra_fast_chargers (accessed on 6 November 2017).
10. Levitan, D. For Electric Car Batteries, the Race for a Rapid Charge, 2012. For Electric Car Batteries, the Race for a Rapid Charge—Yale E360. Available online: http://e360.yale.edu/features/for_electric_car_batteries_the_race_for_a_rapid_charge (accessed on 6 November 2017).
11. Lee, W.Y.; Huh, J.; Choi, S.Y.; Thai, X.V.; Kim, J.H.; Al-Amman, E.A.; El-Kady, M.A.; Rim, C.T. Finite-Width Magnetic Mirror Models of Mono and Dual Coils for Wireless Electric Vehicles. *IEEE Trans. Power Electron.* **2013**, *28*, 1413–1428. [[CrossRef](#)]
12. Ko, Y.D.; Jang, Y.J. The Optimal System Design of the Online Electric Vehicle Utilizing Wireless Power Transmission Technology. *IEEE Trans. Intell. Transp. Syst.* **2013**, *14*, 1255–1265. [[CrossRef](#)]
13. Jang, Y.J.; Suh, E.S.; Kim, J.W. System Architecture and Mathematical Models of Electric Transit Bus System Utilizing Wireless Power Transfer Technology. *IEEE Syst. J.* **2016**, *10*, 495–506. [[CrossRef](#)]
14. Huh, J.; Lee, S.W.; Lee, W.Y.; Cho, G.H.; Rim, C.T. Narrow-Width Inductive Power Transfer System for Online Electrical Vehicles. *IEEE Trans. Power Electron.* **2011**, *26*, 3666–3679. [[CrossRef](#)]

15. Onar, O.C.; Miller, J.M.; Campbell, S.L.; Coomer, C.; White, C.P.; Seiber, L.E. A Novel Wireless Power Transfer for in-Motion EV/PHEV Charging. In Proceedings of the 2013 Twenty-Eighth Annual IEEE Applied Power Electronics Conference and Exposition (APEC), Long Beach, CA, USA, 17–21 March 2013; pp. 3073–3080.
16. Miller, J.M.; Jones, P.T.; Li, J.; Onar, O.C. Ornl Experience and Challenges Facing Dynamic Wireless Power Charging of EV's. *IEEE Circuits Syst. Mag.* **2015**, *15*, 40–53. [[CrossRef](#)]
17. Lee, K.; Pantic, Z.; Lukic, S.M. Reflexive Field Containment in Dynamic Inductive Power Transfer Systems. *IEEE Trans. Power Electron.* **2014**, *29*, 4592–4602. [[CrossRef](#)]
18. Zhao, J.; Cai, T.; Duan, S.; Feng, H.; Chen, C.; Zhang, X. A General Design Method of Primary Compensation Network for Dynamic WPT System Maintaining Stable Transmission Power. *IEEE Trans. Power Electron.* **2016**, *31*, 8343–8358. [[CrossRef](#)]
19. Miller, J.M.; Onar, O.C.; White, C.; Campbell, S.; Coomer, C.; Seiber, L.; Sepe, R.; Steyerl, A. Demonstrating Dynamic Wireless Charging of an Electric Vehicle: The Benefit of Electrochemical Capacitor Smoothing. *IEEE Power Electron. Mag.* **2014**, *1*, 12–24. [[CrossRef](#)]
20. Covic, G.A.; Boys, J.T.; Kissin, M.L.G.; Lu, H.G. A Three-Phase Inductive Power Transfer System for Roadway-Powered Vehicles. *IEEE Trans. Ind. Electron.* **2007**, *54*, 3370–3378. [[CrossRef](#)]
21. Pacini, A.; Mastri, F.; Trevisan, R.; Masotti, D.; Costanzo, A. Geometry Optimization of Sliding Inductive Links for Position-Independent Wireless Power Transfer. In Proceedings of the 2016 IEEE MTT-S International Microwave Symposium (IMS), San Francisco, CA, USA, 22–27 May 2016; pp. 1–4.
22. Mou, X.; Groling, O.; Sun, H. Energy-Efficient and Adaptive Design for Wireless Power Transfer in Electric Vehicles. *IEEE Trans. Ind. Electron.* **2017**, *64*, 7250–7260. [[CrossRef](#)]
23. Zhang, Z.; Chau, K.T. Homogeneous Wireless Power Transfer for Move-and-Charge. *IEEE Trans. Power Electron.* **2015**, *30*, 6213–6220. [[CrossRef](#)]
24. Zhu, Q.; Wang, L.; Guo, Y.; Liao, C.; Li, F. Applying LCC Compensation Network to Dynamic Wireless EV Charging System. *IEEE Trans. Ind. Electron.* **2016**, *63*, 6557–6567. [[CrossRef](#)]
25. Lu, F.; Zhang, H.; Hofmann, H.; Mi, C.C. A Dynamic Charging System with Reduced Output Power Pulsation for Electric Vehicles. *IEEE Trans. Ind. Electron.* **2016**, *63*, 6580–6590. [[CrossRef](#)]
26. Boys, J.T.; Covic, G.A. The Inductive Power Transfer Story at the University of Auckland. *IEEE Circuits Syst. Mag.* **2015**, *15*, 6–27. [[CrossRef](#)]
27. Erickson, R.W.; Maksimovic, D. *Fundamentals of Power Electronics*; Springer: Berlin, Germany, 2001.
28. Park, C.; Lee, S.; Jeong, S.Y.; Cho, G.; Rim, C.T. Uniform Power I-Type Inductive Power Transfer System with DQ-Power Supply Rails for On-Line Electric Vehicles. *IEEE Trans. Ind. Electron.* **2015**, *30*, 6446–6455. [[CrossRef](#)]
29. Zhou, S.; Chris Mi, C. Multi-Paralleled LCC Reactive Power Compensation Networks and their Tuning Method for Electric Vehicle Dynamic Wireless Charging. *IEEE Trans. Ind. Electron.* **2016**, *63*, 6546–6556. [[CrossRef](#)]

